

Influence Analysis and Performance Optimization of a Pneumatic Actuator Exhaust Utilization System

Qihui Yu^{1,2,3} – Fengqi Li^{1,*} – Xin Tan¹

¹ Inner Mongolia University of Science & Technology, Department of Mechanical Engineering, China

² Beijing Key Laboratory, Pneumatic and Thermodynamic Energy Storage and Supply, China

³ University of Nottingham, Department of Mechanical, Materials and Manufacturing Engineering, UK

Due to the loss of exhaust energy, the compressed air energy utilization efficiency in pneumatics system is low. To realize the recovery and utilization of cylinder compressed air, a new type of compressed air utilization system is proposed, and the composition and working principle of the system are introduced. According to the working process of the system, the mathematical model of the system is established by using equations such as energy equation and gas state equation. The model is simulated by MATLAB/Simulink tools, and the correctness of the mathematical model is verified by experiments. The mathematical models are converted into dimensionless models, and the main parameters affecting the system's operating characteristics are obtained through model simulation analysis. The influencing parameters are optimized by using the analytic hierarchy process and the grey correlation analysis method, and the exhaust utilization efficiency of the system is 34.7 % under the optimal parameter combination. To further utilize the compressed air expansion, the opening and closing time of the solenoid valve was controlled to study the energy-saving effect of the system. The study found that when the initial pressure of the compressed air supply tank was set to 0.5 MPa, 0.6 MPa, and 0.7 MPa, the maximum energy saving efficiency was 23.25 %, 24.99 %, and 26.12 %, respectively. When the volume of the compressed air supply tank is set to 0.8 L, 1 L, and 1.2 L, the maximum energy-saving efficiency is 30.01 %, 24.99 %, and 21.51 %, respectively. This paper provides a new technical scheme for compressed air recovery and reuse, as well as a theoretical basis for the control of subsequent compressed air utilization systems.

Keywords: pneumatic system, exhaust utilization, analysis, characteristic, energy saving

Highlights

- An air exhaust utilization loop is proposed, which can recycle the air exhaust to realize energy savings.
- The speed of piston movement and the efficiency of exhaust gas utilization determine the performance of the system.
- The multi-objective parameters are optimized to keep the system stable and good performance.
- Controlling the on-off time of the solenoid valve can further improve the efficiency of gas utilization.

0 INTRODUCTION

The pneumatic system has the characteristics of low-cost, high-strength ratio, convenient maintenance, cleanliness and environmental protection, and high safety [1] to [4]. However, compressed air is expensive to produce and is one of the most expensive energy carriers [5]. Research has found that the actual energy efficiency of some pneumatic systems is low, or even 80 % of the energy will be wasted in the form of heat or other energy in the worst case, which increases the application cost of pneumatic systems [6]. Developing and researching the energy savings of pneumatic systems are urgent tasks.

In recent years, some researchers have changed and optimized the structure of the pneumatic circuit to improve its energy efficiency. Du et al. [7] proposed a bridge-type energy-saving loop that fully utilizes the expansion energy to do work, and significantly improved the system energy efficiency by 50 % to 70 % through algorithm optimization control. After that, Du et al. [8] used a valve to connect the two chambers of the cylinder to improve the bridge circuit

and optimized the control through the finite element configuration method and the interior point method, which could achieve 55 % to 87 % of air energy saving and the cylinder runs more smoothly. Yang et al. [9] and [10] proposed a novel energy recovery booster valve (BVER) and studied its energy efficiency by introducing the concept of aerodynamics. Based on the thermodynamics of metamorphic compressed air, the energy efficiency evaluation and pressure response model of BVER is proposed, which increases the boost ratio by 15 % to 20 %, and the efficiency can be increased by 5 % to 10 % depending on the supply pressure. Endler et al. [11] added a quick-acting on-off valve to the circuit to reduce the impact of external load on compressed air consumption and proposed a compressed air energy-saving decision-making algorithm based on differential pressure and control signals. The research results show that compressed air consumption can be reduced by 47 % to 54 %. Shi et al. [12] and Shi and Cai [13] proposed an expansion energy booster, which cuts off the air supply before the piston moves to the end of the stroke and uses the air expansion to drive the remaining stroke to

achieve energy savings. The SMC company proposes a product that applies the air-saving circuit. It cooperates with the cylinder through the valve and uses the compressed air in the exhaust chamber of the cylinder as the power source when the piston rod retracts to achieve the effect of energy saving, which reduces the air consumption by 45 % compared with the general circuit [14]. For the horizontal installation of the cylinder, Beater [15] adds a pressure-reducing valve to the circuit to reduce the consumption of compressed air by controlling the air supply pressure and shows that the use of this circuit can save 25 % of compressed air. Doll et al. [16] and Doll and Sawodny [17] took full advantage of the expansion energy by controlling five reversing valves, and the studies show that the circuit can save 85 % of the air under optimal conditions. Some scholars make full use of exhaust energy in the form of energy conversion. Cummins recovers energy and stores strain energy with a rubber inner bladder [18]. Luo et al. [19] adopt a closed-loop coordinated control strategy to convert exhaust energy into electrical energy for reuse by utilizing scroll expansion technology.

There are two ways to improve compressed air energy efficiency: changing the structure of the optimized pneumatic circuit and converting the energy of the compressed air. However, the former has a narrow application range and is difficult to control, and the latter has higher requirements on the

conversion device and larger energy loss. In most conventional pneumatic circuits, the energy contained in the compressed air is rarely used efficiently. The method of recovering and utilizing compressed air is simple and easy to control and is an effective way to improve energy efficiency.

In some circuits for compressed air recovery and utilization, the two processes of recovery and utilization cannot be applied to the same scene, resulting in wasted compressed air energy. In view of the above problems, this paper proposes a pneumatic actuator exhaust utilization circuit and introduces the system composition and working principle. Secondly, the mathematical model of the system is established and an experimental platform is built, and the model is verified with experiments. Afterward, through a dimensionless model, the main parameters affecting the performance of the system are studied and optimized. Finally, by controlling the opening and closing time of the solenoid valve, the further utilization of the compressed air expansion energy is studied, which lays a good theoretical foundation for the next step to efficiently control the pneumatic system.

1 SYSTEM COMPOSITION AND WORKING PRINCIPLE

Fig. 1 shows the circuit diagram of the compressed air utilization system. It is mainly composed of the

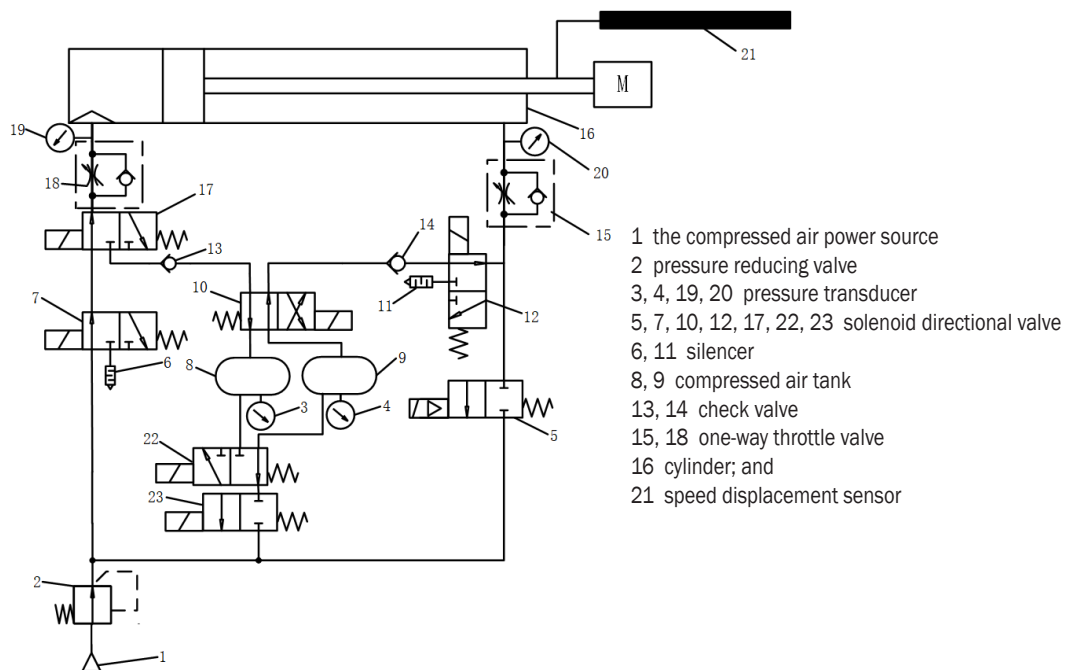


Fig. 1. Exhaust utilization circuit

compressed air source, cylinder, compressed air tank, directional valve, one-way valve, etc. The rod-less chamber of the cylinder is named chamber *a*, the rod chamber is named as chamber *b*, the compressed air tank connected with the chamber *a* is a recycle compressed air tank (*tank1*), and the compressed air tank connected with the chamber *b* is a compressed air supply tank (*tank2*). The pressure of chamber *a*, chamber *b*, *tank1* and *tank2* are named by p_a , p_b , p_{tank1} , p_{tank2} . To study the influence of the relationship between the pressure in the compressed air tank and the cylinder chamber on the performance of the system, define the pressure ratio $\lambda_1 = p_a/p_{tank1}$ as the recovery switching criterion, and $\lambda_2 = p_{tank2}/p_b$ as the supply switching criterion. The principle of a pneumatic actuator exhaust utilization system is as follows.

When the piston rod is extended, the compressed air energy source 1 supplies compressed air to chamber *a*, the released compressed air is adjusted by valve 2, and flows into cylinder chamber *a* after passing through valve 7, valve 17 and valve 18, and drives the cylinder to the right, the compressed air in the chamber *b* is discharged into the environment through valve 15 and valve 12.

When the piston rod is retracted, *tank2* is used as an energy source to supply compressed air to chamber *b* through valve 14, valve 10, valve 12, and valve 15 when $p_{tank2}/p_b > \lambda_2$. If $p_{tank2}/p_b < \lambda_2$, the compressed air energy source 1 is adjusted by valve 2, and the compressed air is supplied to chamber *b* through valve 5 and *t* valve 15. If $p_a/p_{tank1} > \lambda_1$, the compressed air in chamber *a* flows into the recovery compressed air tank through valve 18, valve 17, and valve 13. If $p_a/p_{tank1} < \lambda_1$, Then the compressed air in chamber *a* is discharged into the environment through valve 18, valve 17, and valve 7.

When the recovery process is completed, but the energy is not enough to drive the movement of the piston rod, compressed air energy source 1 is used to pressurize the compressed air tank through electromagnetic reversing valve 21 and valve 22 to meet the requirements.

2 EXPERIMENTAL VERIFICATION OF MATHEMATICAL MODELS

2.1 Mathematical Models

To simplify the calculation, the following assumptions are proposed: (1) The compressed air in the loop follows the ideal compressed air law; (2) The compressed air source is a stable pressure source,

there is no leakage in the system, and the effective area of the inlet and exhaust ports is the same; (3) The compressed air flows into a stable one-dimensional state; (4) The supply compressed air temperature is the same as the atmospheric temperature; (5) The initial pressure of *tank2* is a fixed value.

2.1.1 Energy Equation

Chambers *a* and *b* do not admit compressed air at the same time; according to [20], the energy equation of chambers *a* or *b* can be described as follows :

$$C_v m_i \frac{dT_i}{dt} = (S_i h_i + C_v G_i)(T_e - T_i) + R G_i T_i - p_i A_i u, \quad (1)$$

$$C_v m_i \frac{dT_i}{dt} = S_i h_i (T_e - T_i) + R G_i T_i - p_i A_i u, \quad (2)$$

where, C_v is the constant volume specific heat, [J/(kg·K)], m is compressed air mass, [kg], T is the temperature, [K], T_e is the atmospheric temperature, [K], S is the heat exchange area, [m²], h is the heat exchange coefficient, [W/(m²K)], R is the compressed air constant, [J/(kg·K)], G is the mass flow rate of the compressed air, [kg/s], p is the pressure, [MPa], A is the area, [m²], and u is the speed of piston movement, [m/s]. Subscript *i* represents *a* or *b*.

The energy equation of tank can be described as follows [21]:

$$\frac{dT_j}{dt} = \frac{RT_j}{C_v p_j V_j} [G_j C_p T_u - G_j C_v T_j + h_j S_j (T_e - T_j)], \quad (3)$$

where, V is the volume, [m³]. Subscript *j* represents *tank1* or *tank2*.

2.1.2 Mass Flow Equation

The mass flow equations of chambers *a*, *b*, *tank1* and *tank2* can be expressed as follows:

$$G_{i,j} = \begin{cases} \frac{A_e p_u D}{\sqrt{T_u}} & \frac{p_d}{p_u} \leq b \\ \frac{A_e p_u B}{\sqrt{T_u}} \varphi(p_d, p_u) & \frac{p_d}{p_u} \leq b \end{cases}, \quad (4)$$

where

$$\varphi(p_d, p_u) = \left(\frac{p_d}{p_u}\right)^{\frac{2}{k}} - \left(\frac{p_d}{p_u}\right)^{\frac{k+1}{k}}, \quad (5)$$

$$B = \sqrt{\frac{2K}{R(k-1)}}, \quad (6)$$

$$D = \left(\frac{2}{k+1} \right)^{\frac{1}{k-1}} \sqrt{\frac{2k}{R(k+1)}}, \quad (7)$$

where, p_d and p_u are the downstream and upstream pressures, respectively, [MPa], A_e is the effective area of the intake and exhaust ports, [m²], T_u is the upstream temperature, [K], k is the specific heat ratio, and b is the critical pressure ratio.

2.1.3 Dynamic Equation

The force diagram of the piston is shown in Fig. 2. The equation of motion of the piston can be obtained according to Newton's second law.

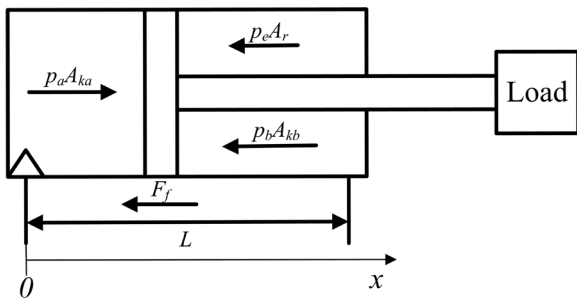


Fig. 2. Movement direction and force diagram of piston

The motion equation of the piston is shown in Eq. (8):

$$\frac{d^2 x}{dt^2} = \begin{cases} \frac{1}{M} (p_a A_{ka} - p_b A_{kb} - p_e A_r - F_f) & x \neq n_a, L - n_b \\ 0 & x = n_a, L - n_b \end{cases}, \quad (8)$$

where, M is the mass of load, [kg], L is the cylinder stroke, [m], F_f is the friction, [N], A_{ki} is the effective area of the piston, [m²], p_e is atmospheric pressure, [MPa], A_r is the effective area of the piston rod, [m²]; n is the dead zone displacement, [m].

The friction force of the pneumatic system includes many factors. The composite model proposed by Canudas in 1995 can comprehensively reflect the friction characteristics of the contact surface of the pneumatic system under lubrication conditions [22] and [23]. In this paper, the composite model described by Eq. (9) is used as the mathematical model of the friction force of the cylinder.

$$F_f = \begin{cases} \alpha \cdot u + \left[F_c + (F_s - F_c) e^{-\left(\frac{u}{u_s}\right)^\delta} \right] \operatorname{sgn}(u) & u \leq u_e \\ \mu \cdot u & u > u_e \end{cases}, \quad (9)$$

where, α is the cylinder viscosity coefficient, [N/(m/s)], F_c is the coulomb friction force, [N], F_s is the maximum static friction force, [N], μ is the

dynamic friction factor; u_s is the Stribeck velocity, [m/s], δ is an arbitrary index (0.5 to 2), and u_e is the critical speed, [m/s].

2.1.4 Equation of Compressed Air State

According to the pressure changes of the two chambers of the cylinder, the state equations of chambers a and b can be derived as:

$$\frac{dp_i}{dt} = \frac{1}{V_i} \left(RT_i G_i - p_i A_i u + \frac{p_i V_i}{T_i} \cdot \frac{dT_i}{dt} \right). \quad (10)$$

The equation of the state of the compressed air in the compressed air tank is expressed as follows [24]:

$$\frac{dp_j}{dt} = \frac{R}{C_v V_j} \left[G_j C_p T_u + h_j S_{hj} (T_e - T_j) \right], \quad (11)$$

where S_h is the surface area of the inner wall of the tank chamber, [m²].

2.1.5 Basic Parameters

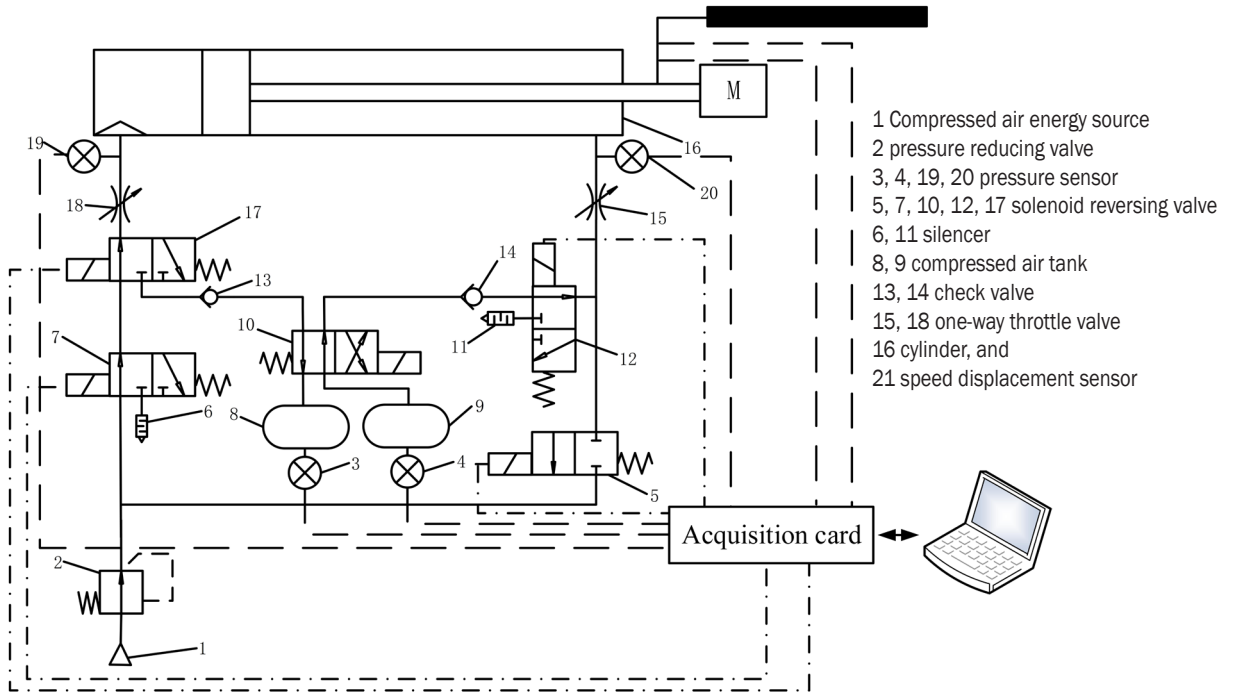
The basic parameters are shown in Table 1, and the above mathematical model is constructed using MATLAB/Simulink. B is the value of process quantity in the simulation process.

Table 1. Basic parameters of the system

| Parameter | Value | Parameter | Value | Parameter | Value |
|--------------|--------|--------------------|--------|--------------|--------|
| M , [kg] | 5 | V_{tank1} , [L] | 1 | B | 50 |
| L , [mm] | 200 | V_{tank2} , [L] | 1 | F_c , [N] | 8 |
| D , [mm] | 63 | C_v , [J/(kg·K)] | 718 | F_s , [N] | 50 |
| d , [mm] | 20 | C_p , [J/(kg·K)] | 1005 | T_e , [K] | 293 |
| p_s , [Pa] | 600000 | R , [J/(kg·K)] | 287 | P_0 , [Pa] | 600000 |
| p_e , [Pa] | 101300 | b | 0.5283 | | |

2.2 Experimental Verification

In order to verify the correctness of the mathematical model, an experimental platform for exhaust utilization was built. The compressed air preparation unit consists of a regulator, a filter, and a lubrication control. Its main function is to reduce the pressure to a fixed value. Four pressure sensors are used to monitor the pressure in chamber a , chamber b , $tank1$, and $tank2$. Displacement sensors are used to monitor piston displacement. A force sensor is used to measure the output force of the pneumatic cylinder; an NI data acquisition card and computer are used to obtain experimental data.



- 1 Compressed air energy source
- 2 pressure reducing valve
- 3, 4, 19, 20 pressure sensor
- 5, 7, 10, 12, 17 solenoid reversing valve
- 6, 11 silencer
- 8, 9 compressed air tank
- 13, 14 check valve
- 15, 18 one-way throttle valve
- 16 cylinder, and
- 21 speed displacement sensor

Fig. 3. Schematic diagram of pneumatic system experiment

The pressure sensor test range is 0 MPa to 1 MPa, and the force sensor test range is 3 N to 3000 N. The measurement accuracy of pressure, displacement, and force are, respectively 1 %, $\pm 5 \mu\text{m}$, and $\pm 0.05 \%$. Therefore, the maximum absolute errors of pressure, displacement and force are 0.01 MPa, $\pm 5 \mu\text{m}$, and $\pm 1.5 \text{ N}$, respectively.

The compressed air source should be turned on, and the pressure in *tank2* set to a fixed value through the regulator. The system uses LabVIEW to control and save the data and realize the return stroke of the cylinder by controlling the four solenoid valves.

Fig. 3 is the experimental schematic diagram of the system, and the experimental platform is shown in Fig. 4. Using the experimental platform, the experimental research on the compressed air utilization system is carried out. The compressed air source pressure is set to 0.6 MPa, the load mass is set to 5 kg. Fig. 5 shows the relationship between some parameters and time in the system.

The performance of the system will be shown by some parameters. Fig. 5 includes the piston displacement, velocity, chamber *a*, chamber *b*, and the changes of two tanks in simulation and experiment, which directly shows the performance of the system.

It can be seen from Fig. 5 that the experimental results and the various parameter curves in the simulation have the same trend of change, the pressure

in chamber *b* rises first, and then decreases. As the pressure in chamber *a* decreases, the pressure in *tank1* first rises and then remains unchanged, and the pressure in *tank2* decreases first, remains unchanged in the middle, and finally decreases again.

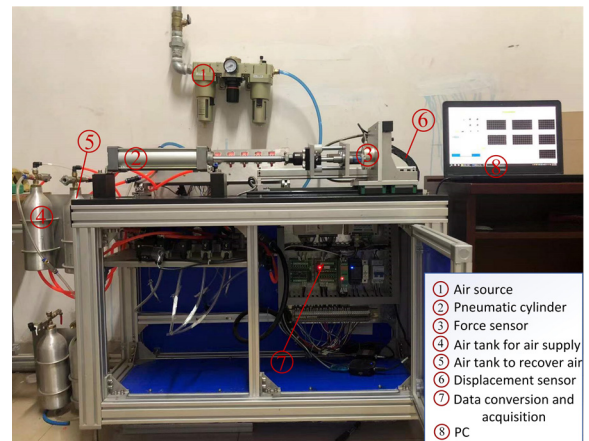


Fig. 4. Experimental platform

- ① Air source
- ② Pneumatic cylinder
- ③ Force sensor
- ④ Air tank for air supply
- ⑤ Air tank to recover air
- ⑥ Displacement sensor
- ⑦ Data conversion and acquisition
- ⑧ PC

There are certain errors in the experimental and simulated values, but the maximum error is within 10 %. The reasons for the error in the analysis may be the estimation of parameters such as friction force in the simulation, the instability of the compressed air source pressure, the existence of compressed air leakage in

the pneumatic circuit, and the expansion energy of the compressed air in the cylinder is ignored. On the basis of previous studies [25], it can be known that the main cause of the error is the instability of gas source pressure. The purpose of this experiment is to explore the influence law of system performance through the general change trend of the curve. Therefore, the

correctness of the model is verified by the comparison of the curve trend between simulation and experiment.

3 SIMULATION ANALYSIS OF DIMENSIONLESS MODELS

To understand the performance changes of the system more objectively, it is necessary to use the dimensionless method to eliminate physical units and study the characteristics of the system. To facilitate the research, the assumptions made in Section 2 also apply to this section. The reference values and the dimensionless variables are shown in Table 2. The basic mathematical model can be made dimensionless as described below.

Table 2. Reference values and dimensionless variables

| Variable | Reference value | Dimensionless variable |
|----------|---------------------------------|------------------------|
| P | p_s | $p^* = p/p_s$ |
| T | $T_p = V_a/(A_e DR)$ | $t^* = t/T_p$ |
| G | $G_{max} = p_s A_e D/T_e$ | $G^* = G/G_{max}$ |
| T | T_e | $T^* = T/T_e$ |
| X | L | $x^* = x/L$ |
| A | A_{ka} | $A^* = A/A_{ka}$ |
| V | V_a | $V^* = V/V_a$ |
| M | $m_{max} = p_s V_a/(R\theta_0)$ | $m^* = m/m_{max}$ |

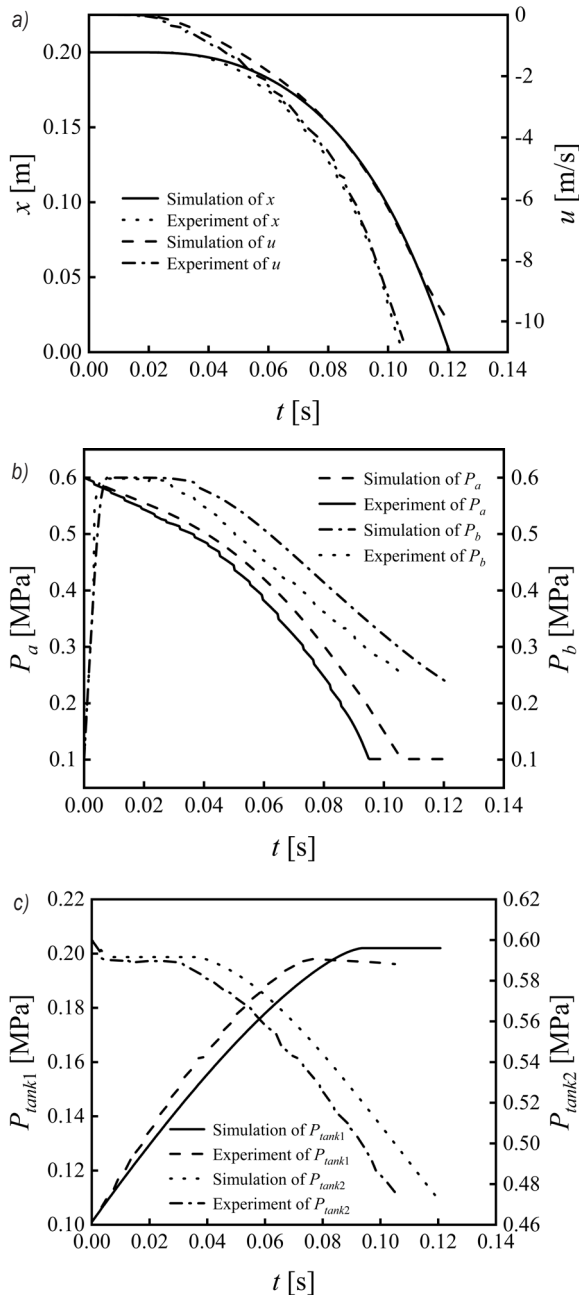


Fig. 5. Comparison of experimental and simulation curves; a) displacement and velocity curve of piston, b) pressure curve of chamber a and b, and c) pressure curve of tank1 and tank2

3.1 Dimensionless Models

3.1.1 Dimensionless Energy Equation

When the compressed air is charged into chamber a or chamber b, its dimensionless energy equation can be expressed as follows:

$$m_i^* \frac{dT_i^*}{dt^*} = \left(\frac{S_i^* K_{ab}}{S_{max}^*} + G_a^* \right) (1 - T_i^*) + (k - 1) (G_i^* - p_i^* A_i^* u_i^*). \quad (12)$$

When the compressed air is discharged from chamber a or chamber b, its dimensionless energy equation can be expressed as follows:

$$m_i^* \frac{dT_i^*}{dt^*} = \frac{S_i^* K_{aa}}{S_{max}^*} (1 - T_i^*) + (k - 1) (p_i^* u_i^* - G_i^* T_i^*). \quad (13)$$

The dimensionless energy equation of the compressed air tank can be expressed as follows:

$$\frac{dT_j^*}{dt^*} = \frac{T_j^*}{p_j^*} \left[(k - T_j^*) G_j^* + K_{aj} (1 - T_j^*) \right], \quad (14)$$

where, K_a is the Kagawa coefficient [25], which represents the degree of heat transfer and is defined by Eqs. (15) and (16).

$$K_{ai} = \frac{T_p}{T_{hi}}, \quad (15)$$

$$K_{aj} = \frac{T_p}{T_{hj}}, \quad (16)$$

$$T_{hi} = \frac{C_v m}{S_{max} h_i}, \quad (17)$$

$$T_{hj} = \frac{C_v m_j}{S_j h_j}, \quad (18)$$

$$S_{max} = 2A_{ka} + 2L\sqrt{\pi A_{ka}}, \quad (19)$$

where, T_h is the thermal equilibrium time constant; T_p is the reference time constant; S_{max} is the maximum heat exchange area of the two chambers of the cylinder, [m²].

The dimensionless maximum heat exchange area of chamber a and b is expressed as follows:

$$S_{max}^* = \frac{S_{max}}{A_{ka}} = 2 + 2L\sqrt{\frac{\pi}{A_{ka}}}. \quad (21)$$

The dimensionless heat exchange area of the $tank1$ and $tank2$ is as follows:

$$S_j^* = \frac{S_j}{A_{ka}} = \frac{2A_j + 2L_j\sqrt{\pi A_j}}{A_{ka}}. \quad (22)$$

3.1.2 Dimensionless Mass Flow Equation

The dimensionless mass flow equation of chamber a or b is expressed as:

$$G_i^* = \begin{cases} \frac{p_d^* A_e^*}{\sqrt{T_u^*}} & \frac{p_d^*}{p_u^*} \leq b \\ \frac{p_u^* B A_e^*}{D \sqrt{T_u^*}} \sqrt{\left(\frac{p_d^*}{p_u^*}\right)^{\frac{2}{k}} - \left(\frac{p_d^*}{p_u^*}\right)^{\frac{k+1}{k}}} & \frac{p_d^*}{p_u^*} \geq b \end{cases}. \quad (23)$$

The dimensionless mass flow equation of $tank1$ is expressed as:

$$G_{tank1}^* = \begin{cases} 1 & p_{tank1}^* \leq b \\ \sqrt{1 - \left(\frac{p_{tank1}^* - b}{1 - b}\right)} & p_{tank1}^* \geq b \end{cases}. \quad (24)$$

The dimensionless mass flow equation of $tank2$ is expressed as:

$$G_{tank2}^* = \begin{cases} \frac{p_{tank2}^*}{\sqrt{T_{tank2}^*}} & p_{tank2}^* \leq b \\ \frac{p_{tank2}^*}{\sqrt{T_{tank2}^*}} \sqrt{1 - \left(\frac{p_{tank2}^* - b}{1 - b}\right)} & p_{tank2}^* \geq b \end{cases}. \quad (25)$$

3.1.3 Dimensionless Motion Equation

The dimensionless motion equation of the piston is described as:

$$\frac{d^2 x^*}{d(t^*)^2} = \begin{cases} \left(\frac{1}{T_f^*}\right)^2 (A_{kb}^* p_b^* - p_a^* - p_e^* A_r^* - F_f^*) & x \neq 0, L \\ 0 & x = 0, L \end{cases}, \quad (26)$$

where, F_f^* is an estimated value that can be calculated by Eq. (27):

$$F_f^* = \begin{cases} F_s^* & u^* = 0 \\ F_c^* + C^* u^* & u^* \neq 0 \end{cases}, \quad (27)$$

where, C^* is the dimensionless viscous friction coefficient which can be described as follows:

$$F_s^* = \frac{F_s}{p_s A_{ka}}, \quad (28)$$

$$F_c^* = \frac{F_c}{p_s A_{ka}}, \quad (29)$$

$$C^* = \frac{C u_0}{p_s A_{ka}}, \quad (30)$$

where, u_0 is the reference speed, [m/s]; p_s is the compressed air source pressure, [MPa].

The dimensionless parameter T_f^* is defined by Eq. (32), and T_f^* corresponds to the J parameter used when selecting the cylinder.

$$T_f^* = \frac{T_f}{T_p}, \quad (31)$$

$$T_f = \sqrt{\frac{ML}{p_s A_{ka}}}. \quad (32)$$

The mathematical relationship between J parameter and T_f^* is shown below:

$$J = \left(\frac{1}{T_f^*}\right)^2. \quad (33)$$

3.1.4 Dimensionless Equation of State

According to the pressure changes of chamber *a* or *b*, dimensionless equation of state is expressed as follows:

$$\frac{dp_i^*}{dt^*} = \frac{G_i^* T_i^* - p_i^* A_i^* u_i^*}{V_i^*} + \frac{p_i^*}{T_i^*} \frac{dT_i^*}{dt^*}. \quad (34)$$

The equation of *tank1* is expressed as follows:

$$\frac{dp_{tank1}^*}{dt^*} = kG_{tank1}^* + K_{a3} (1 - T_{tank1}^*). \quad (35)$$

The equation of *tank2* is expressed as follows:

$$\frac{dp_{tank2}^*}{dt^*} = kG_{tank2}^* p_{tank2}^* \sqrt{T_{tank2}^*} + K_{a4} (1 - T_{tank2}^*). \quad (36)$$

3.2 Dimensionless Simulation Analysis

To explore the relationship between the dimensionless initial pressure of *tank2* and the utilization efficiency of compressed air, the ratio of the initial pressure p_0 of *tank2* to the compressed air source pressure p_s is defined as the dimensionless initial supply pressure of *tank2*, which is expressed as $\beta^* = p_0/p_s$. Table 3 is the reference value of dimensionless parameters.

Based on the simulation program, the variation trend of each dimensionless physical quantity can be obtained by substituting parameters.

Fig. 6 shows the trend of dimensionless parameters over time. It can be seen from Fig. 6a that the piston does not move for an initial period of time. This is because the driving force of the driving chamber during this period is less than the sum of other resistances such as compressed air resistance and friction in the chamber *a*, and the piston is stationary. It can be seen from Fig. 6b that the pressure in chamber *b* first rises and then falls, because the friction force changes from static friction force to kinetic friction force after the piston moves, and the reduction of friction force accelerates the movement of the piston. At this time, the volume of chamber *b* increases, and the intake air volume is less than the increase in the volume of chamber *b*, the compressed air expands, and the pressure decreases. The pressure in chamber *b* does not rise again because the air supply time is short.

It can be seen from Fig. 6c that the pressure in *tank1* first increases and then remains unchanged. This is because the system does not meet the recovery criterion, the compressed air in chamber

a is discharged into the atmosphere, the pressure in *tank1* remains unchanged. The pressure in *tank2* first decreases, then remains unchanged, and then decreases. This is because the system does not meet the air supply criterion, and the air supply from *tank2* is switched to the air supply. Fig. 7a shows the working condition of the recovery part and the pressure in *tank2* remains unchanged. Fig. 7b shows the specific working conditions of the gas supply part.

Table 3. Dimensionless parameter reference value

| Dimensionless parameters | Symbol | Reference value |
|---|---------------|-----------------|
| Dimensionless natural period | T_f^* | 0.0663 |
| Dimensionless static friction | F_s^* | 0.0267 |
| Dimensionless viscous friction coefficient | C^* | 0.0153 |
| Dimensionless piston area of chamber <i>b</i> | A_{kb}^* | 0.8992 |
| Dimensionless Coulomb friction | F_c^* | 0.0043 |
| Effective area of dimensionless compressed air inlet | A_{e2}^* | 1 |
| Kagawa coefficient of chamber <i>a</i> | K_{aa} | 0.0563 |
| Kagawa coefficient of chamber <i>b</i> | K_{ab} | 0.0626 |
| Dimensionless volume of <i>tank1</i> | V_{tank1}^* | 1.604 |
| Dimensionless volume of <i>tank2</i> | V_{tank2}^* | 1.604 |
| Recovery switching criterion | λ_1 | 1 |
| Criteria for compressed air supply switching | λ_2 | 1 |
| Dimensionless initial supply pressure of <i>tank2</i> | β^* | 1 |
| Dimensionless air source pressure | β_s^* | 1 |

4 PERFORMANCE RESEARCH AND PARAMETER OPTIMIZATION

To obtain main influence parameters on efficiency and speed, further research on its speed and efficiency characteristics is essential; it should select the parameters with the high degree of impact, optimize the main performance of the system, and obtain the parameter combination under the optimal conditions.

4.1 Performance Analysis

Piston velocity and exhaust utilization efficiency reflect the main performance of exhaust utilization system, so the parameters affecting piston velocity and exhaust utilization efficiency are studied as dimensionless.

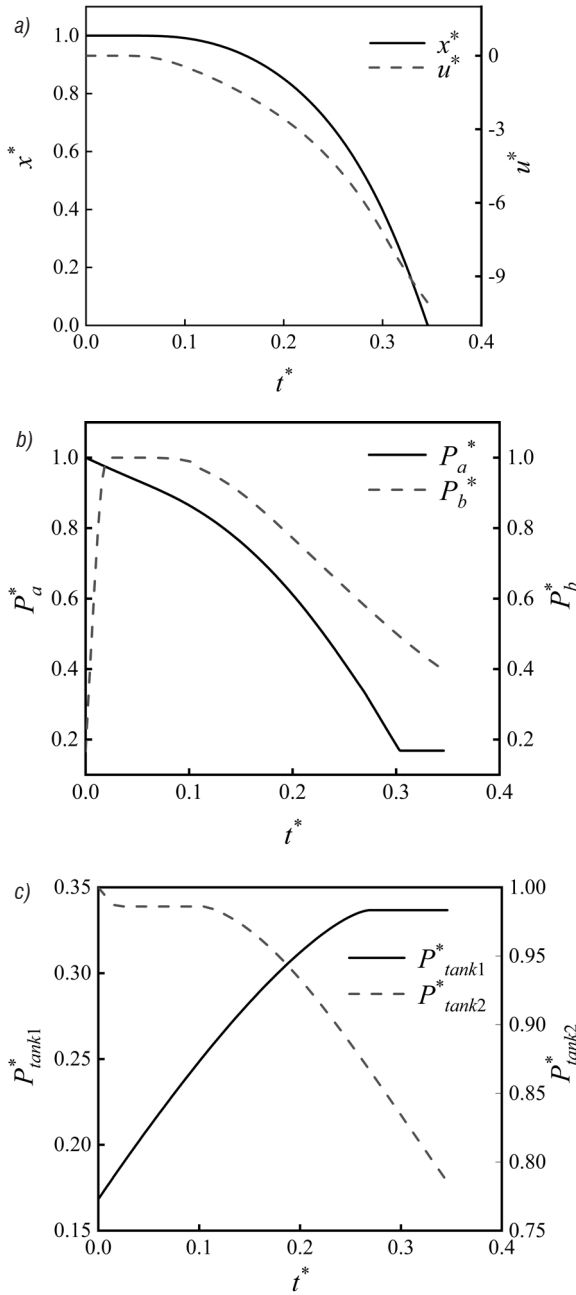


Fig. 6. Simulation curve; a) displacement and velocity curve of piston, b) pressure curve of chamber a and b, c) pressure curve of tank1 and tank2

4.1.1 Dimensionless Speed Analysis

To facilitate the study of the influence of various dimensionless parameters on the speed characteristics of the piston, the dimensionless speed of the piston is defined as:

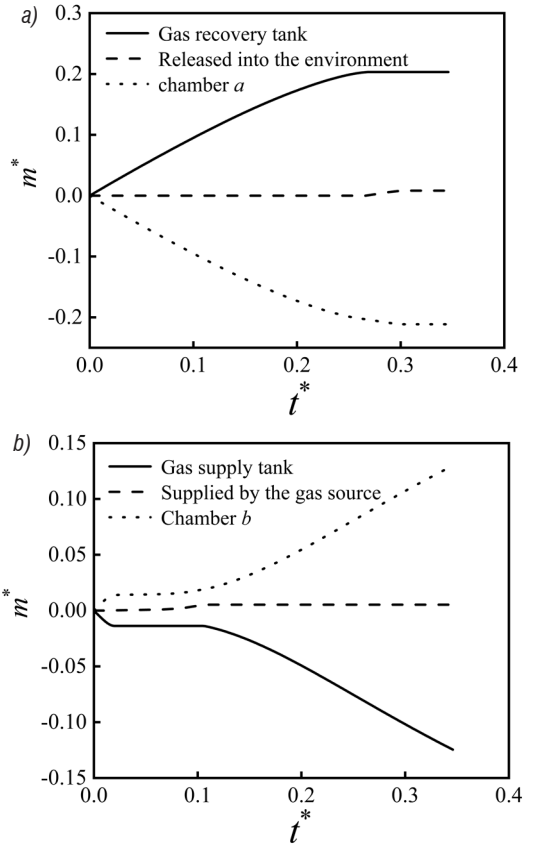


Fig. 7. Change in compressed air mass; a) compressed air mass changes in the recovery part, b) compressed air mass changes in the supply part

$$\bar{u}^* = \frac{\int_0^t u^* dt}{t} \tag{37}$$

The rate of change of dimensionless speed refers to the ratio of a parameter to the sum of the dimensionless average rate of change of all parameters. The sum of the dimensionless average speed change rate can be described as follows:

$$\begin{aligned} \bar{u}_{total-cg} = & \bar{u}_{T_f^*-cg} + \bar{u}_{F_s^*-cg} + \bar{u}_{C^*-cg} + \bar{u}_{A_{kb}^*-cg} + \bar{u}_{F_c^*-cg} \\ & + \bar{u}_{A_{e2}^*-cg} + \bar{u}_{K_{a1}^*-cg} + \bar{u}_{K_{a2}^*-cg} + \bar{u}_{V_{r1}^*-cg} + \bar{u}_{V_{r2}^*-cg} \\ & + \bar{u}_{\lambda_1-cg} + \bar{u}_{\lambda_2-cg} + \bar{u}_{\beta-cg} + \bar{u}_{\beta_s-cg} \end{aligned} \tag{38}$$

It can be seen from Fig. 8 that u^* is mainly affected by T_f^* , A_{e2}^* , A_{kb}^* , β^* , and the rate of change of these parameters are respectively 23.57 %, 23.48 %, 36.42 %, and 7.87 %.

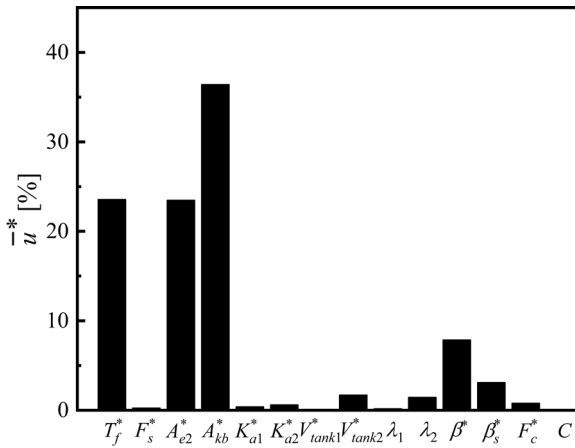


Fig. 8. Rate of change of speed

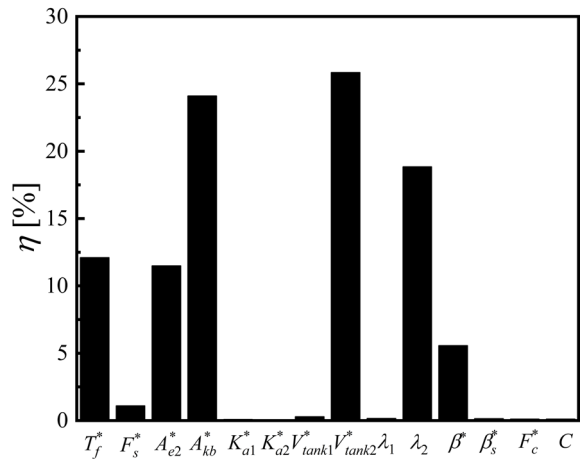


Fig. 9. The rate of change of the dimensionless efficiency of each parameter

4.1.2 Dimensionless Efficiency Analysis

At the initial moment of compressed air reuse, the pressure in the exhaust chamber of the cylinder can be approximated as the supply pressure. Because the temperature change in the pipeline is difficult to measure and the compressed air tank is large when the system is working, the change in the compressed air flow process is not considered, and only the enthalpy of the compressed air is considered. For the calculation of air volume and pressurized compressed air energy in standard state, please refer to the relevant literature [26] and [27].

The efficiency of compressed air utilization can be calculated by:

$$\eta = \frac{E_c^* - E_s^*}{E_c^*} \times 100\%, \quad (39)$$

where, E_c^* is the dimensionless energy at the beginning of the return trip, E_s^* is the dimensionless energy at the end of the return trip.

Through the model established by the above process, in the research process, the value of a single parameter is changed to obtain the influence rate of the change of each parameter on the compressed air utilization efficiency. In order to evaluate the characteristics of compressed air reuse efficiency more objectively, the dimensionless average efficiency is defined as follows:

$$\bar{\eta} = \frac{\int_0^t \eta dt}{t}. \quad (40)$$

The change rate of dimensionless efficiency refers to the ratio of a parameter to the sum of the dimensionless average efficiency change rates of all

parameters. The sum of the dimensionless average efficiency change rate can be described as follows:

$$\begin{aligned} \bar{\eta}_{total-cg} = & \bar{\eta}_{T_f^*-cg} + \bar{\eta}_{F_s^*-cg} + \bar{\eta}_{C^*-cg} + \bar{\eta}_{A_{kb}^*-cg} + \bar{\eta}_{F_c^*-cg} \\ & + \bar{\eta}_{A_{e2}^*-cg} + \bar{\eta}_{K_{a1}^*-cg} + \bar{\eta}_{K_{a2}^*-cg} + \bar{\eta}_{V_{tank1}^*-cg} + \bar{\eta}_{V_{tank2}^*-cg} \\ & + \bar{\eta}_{\lambda_1-cg} + \bar{\eta}_{\lambda_2-cg} + \bar{\eta}_{\beta-cg} + \bar{\eta}_{\beta_s-cg}. \end{aligned} \quad (41)$$

Fig. 9 describes the change rate of the dimensionless efficiency of each parameter.

It can be seen from Fig. 9 that the compressed air utilization efficiency is mainly affected by V_{tank2}^* , A_{kb}^* , λ_2 , T_f^* and A_{e2}^* . The change rates of these parameters were 25.84 %, 24.1 %, 18.84 %, 12.1 %, and 11.49 %.

4.2 Parameter Optimization

Optimizing the main parameters that affect the performance of the system can further improve the effect of energy saving. It can be seen from the above research that the dimensionless piston speed and compressed air utilization efficiency are mainly affected by T_f^* , A_{e2}^* , A_{kb}^* , λ_2 , β^* and V_{tank2}^* . The orthogonal experiments should be designed in the optimization process, and the grey relational analysis method used to optimize the key parameters that affect the performance of the system.

The overall optimization objective function can be defined as follows:

$$f(x) = \alpha_1 u + \alpha_2 V_{tank2} + \alpha_3 \eta, \quad (42)$$

where, α_1 is the speed weighting factor, α_2 is the reused compressed air tank volume weighting factor, and α_3 is the reuse efficiency weighting factor.

There are three weighting factors in the objective function, and the importance of the three factors is different. The analytic hierarchy process can transform multi-objective and multi-criteria problems into multi-level single-objective problems, and the results are simpler and clearer. Here we choose the analytic hierarchy process to obtain the weighting factor. By dividing the importance of the factors, the weighting factors of the specific objective function as shown in Table 4 are obtained by calculation.

Therefore, the weighting factor of the objective function is $\alpha = (\alpha_1, \alpha_2, \alpha_3)^T = (0.5, 0.2, 0.3)^T$.

Table 4. Objective function weighting factors

| Parameter | u | V_{tank2} | η | $\sum_m \alpha_{mn}$ | $\frac{\sum_m \alpha_{mn}}{\sum_n \sum_m \alpha_{mn}}$ |
|-----------------------------|-----|-------------|--------|----------------------|--|
| u | 1 | 5/2 | 5/3 | 31/6 | 0.5 |
| V_{tank2} | 2/5 | 1 | 2/3 | 31/15 | 0.2 |
| η | 3/5 | 3/2 | 1 | 31/10 | 0.3 |
| $\sum_n \sum_m \alpha_{mn}$ | | | | 31/3 | 1 |

Table 5. Parameter boundary value

| | Parameter | | | | | |
|----------------|-----------|-----------------------------|-----------------------------|-------------|---------|-----------------|
| Boundary value | T_f [s] | A_{e2} [mm ²] | A_{kb} [mm ²] | λ_2 | β | V_{tank2} [L] |
| Lower boundary | 0.0103 | 50.27 | 2626.37 | 0.8 | 0.4 | 0.8 |
| Upper boundary | 0.0326 | 176.72 | 3004.15 | 1.2 | 0.8 | 1.2 |

The most representative and smallest combination of all combinations of experimental factors is selected by orthogonal experiment method, and part of the experimental results is used to characterize all experimental conditions. When the value of V_{tank2} is set within 0.2 L from the initial value, the energy in *tank2* can meet the system requirements, and the compressed air recovery and utilization process will not be complicated. Values of λ_2 and β other than 0.2 from the initial value will have a greater impact on the speed of the piston, so λ_2 and β should be taken within 0.2 of the initial value. The upper and lower boundary values of T_f , A_{e2} , and A_{kb} are calculated according to the values of other parameters. Table 5 shows the upper and lower boundary values of each parameter.

Five values are selected for each of the six parameters, and the $L_{25}(5^6)$ orthogonal table is used to obtain the combination of parameters. The parameters' values are shown in Table 6.

Table 6. Parameters combinations

| No. | Parameter | | | | | |
|-----|-----------|-----------------------------|-----------------------------|-------------|---------|-----------------|
| | T_f [s] | A_{e2} [mm ²] | A_{kb} [mm ²] | λ_2 | β | V_{tank2} [L] |
| 1 | 0.0103 | 50.27 | 2626.37 | 0.8 | 0.4 | 0.8 |
| 2 | 0.0103 | 95.00 | 2410.39 | 0.9 | 0.5 | 0.9 |
| 3 | 0.0103 | 113.10 | 2803.12 | 1 | 0.6 | 1 |
| 4 | 0.0103 | 153.94 | 2916.18 | 1.1 | 0.7 | 1.1 |
| 5 | 0.0103 | 176.72 | 3004.15 | 1.2 | 0.8 | 1.2 |
| 6 | 0.0146 | 50.27 | 2410.39 | 1 | 0.7 | 1.1 |
| 7 | 0.0146 | 95.00 | 2803.12 | 1.1 | 0.8 | 1.2 |
| 8 | 0.0146 | 113.10 | 2916.18 | 1.2 | 0.4 | 0.8 |
| 9 | 0.0146 | 153.94 | 3004.15 | 0.8 | 0.5 | 0.9 |
| 10 | 0.0146 | 176.72 | 2626.37 | 0.9 | 0.6 | 1 |
| 11 | 0.0207 | 50.27 | 2803.12 | 1.2 | 0.5 | 0.9 |
| 12 | 0.0207 | 95.00 | 2916.18 | 0.8 | 0.6 | 1 |
| 13 | 0.0207 | 113.10 | 3004.15 | 0.9 | 0.7 | 1.1 |
| 14 | 0.0207 | 153.94 | 2626.37 | 1 | 0.8 | 1.2 |
| 15 | 0.0207 | 176.72 | 2410.39 | 1.1 | 0.4 | 0.8 |
| 16 | 0.0292 | 50.27 | 2916.18 | 0.9 | 0.8 | 1.2 |
| 17 | 0.0292 | 95.00 | 3004.15 | 1 | 0.4 | 0.8 |
| 18 | 0.0292 | 113.10 | 2626.37 | 1.1 | 0.5 | 0.9 |
| 19 | 0.0292 | 153.94 | 2410.39 | 1.2 | 0.6 | 1 |
| 20 | 0.0292 | 176.72 | 2803.12 | 0.8 | 0.7 | 1.1 |
| 21 | 0.0326 | 50.27 | 3004.15 | 1.2 | 0.6 | 1 |
| 22 | 0.0326 | 95.00 | 2626.37 | 1.1 | 0.7 | 1.1 |
| 23 | 0.0326 | 113.10 | 2410.39 | 0.8 | 0.8 | 1.2 |
| 24 | 0.0326 | 153.94 | 2803.12 | 0.9 | 0.4 | 0.8 |
| 25 | 0.0326 | 176.72 | 2916.18 | 1 | 0.5 | 0.9 |

The parameters' combinations are substituted into the simulation model to obtain the value of each objective function, and the results are combined and calculated by the grey correlation degree method, and the value of the correlation degree is used to evaluate the pros and cons of these combinations, so as to obtain the optimal result. The corresponding parameter combinations are shown in Table 7. The optimal result is brought into the model simulation, and the single exhaust utilization efficiency of the system is 34.7 %.

Table 7. Optimized parameters

| Parameter | | | | | |
|-----------|-----------------------------|-----------------------------|-------------|---------|-----------------|
| T_f [s] | A_{e2} [mm ²] | A_{kb} [mm ²] | λ_2 | β | V_{tank2} [L] |
| 0.0292 | 176.72 | 2803.12 | 0.8 | 0.7 | 1.1 |

5 RESEARCH ON ENERGY-SAVING UTILIZATION OF EXPANSION ENERGY

In the above research process, only the transmission energy of the compressed air is used, while the

expansion energy of the compressed air is hardly used, which results in a waste of compressed air energy. To make use of the expansion of the compressed air, the opening and closing sequence of the solenoid valve is changed to control the air supply time to the chamber *b*, so that the air is sufficiently expanded to push the piston back. During the return process, the energy change of the pressurized compressed air in *tank2* and the speed of the piston are studied.

5.1 Solenoid Valve Working Status

Fig. 10 shows the value opening and closing sequence diagrams of the four solenoid valves under the basic operating conditions, where *u1*, *u2*, *u3*, and *u4* are solenoid valve 7, solenoid valve 17, solenoid valve 12, and solenoid valve 5, respectively.

The 0 state in Fig. 10 indicates that the solenoid valve is de-energized and closed, and the 1 state indicates that the solenoid valve is energized and opened. In the actual working process, the solenoid valve does not act instantaneously when the solenoid valve is disconnected and closed; there is a 10 ms response time.

5.2 System Performance Analysis of Variable Initial Pressure of *tank2*

The volume of *tank2* is 1 L, and the initial pressure of *tank2* is 0.5 MPa, 0.6 MPa, and 0.7 MPa, respectively, and cut off the compressed air supply of *tank2* to the chamber *b* at 0.06 s, 0.07 s, 0.08 s, 0.09 s and 0.1 s, respectively. The expansion of the compressed air in the chamber *b* can be utilized in the subsequent time.

Fig. 11 shows the working conditions of the solenoid valve and the change of the pressure in *tank2* in different working conditions.

It can be seen from Fig. 12 that when the initial pressure of *tank2* is constant, the energy saving efficiency decreases with the increase of the time of cutting off *tank2*, and when the time of cutting off *tank2* is fixed, the energy saving efficiency decreases with the increase of the initial pressure of *tank2*. However, when the time of cutting off the *tank2* is 0.06 s, the energy saving efficiency increases with the increase of the initial pressure, and the maximum is 26.12 %. The reason may be that when the initial pressure of the *tank2* is large, the time of cutting off the *tank2* has a great influence on the energy saving efficiency.

It can be seen from Fig. 13 that when the initial pressure of *tank2* is constant, the average piston velocity increases with the increase of the time of cutting off *tank2*, and when the time of cutting off *tank2* is fixed, the average velocity of piston increases with the increase of the initial pressure of *tank2*. In the working process of the system, it is necessary to avoid cutting off the *tank2* too early to affect the normal operation of the system.

When the volume of *tank2* is 1 L, in order to improve the energy saving efficiency of the system and not make the piston speed too low affect the operation of the system, it is suggested that the time of cutting off *tank2* is 0.06 s to 0.08 s and the initial pressure of *tank2* is 0.6 MPa to 0.7 MPa.

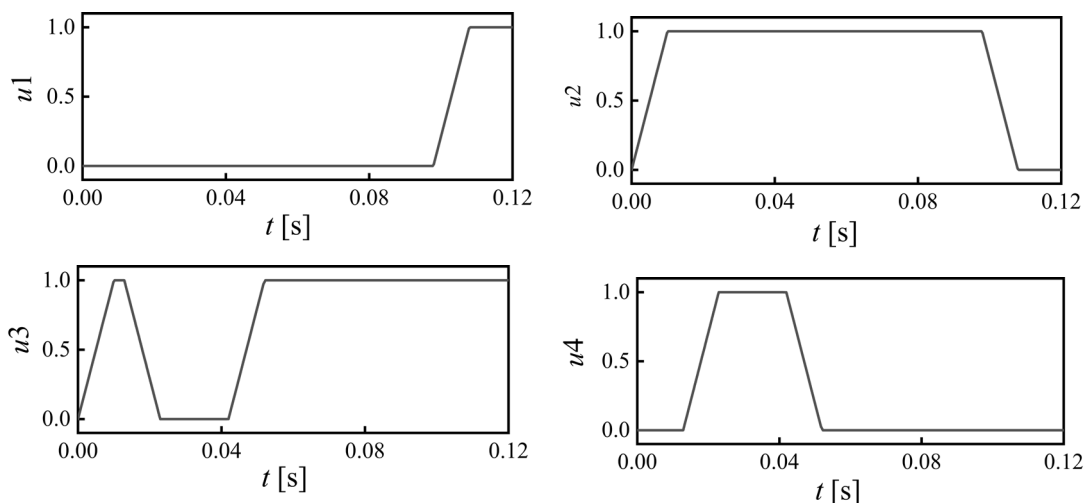


Fig. 10. Working condition of solenoid valve

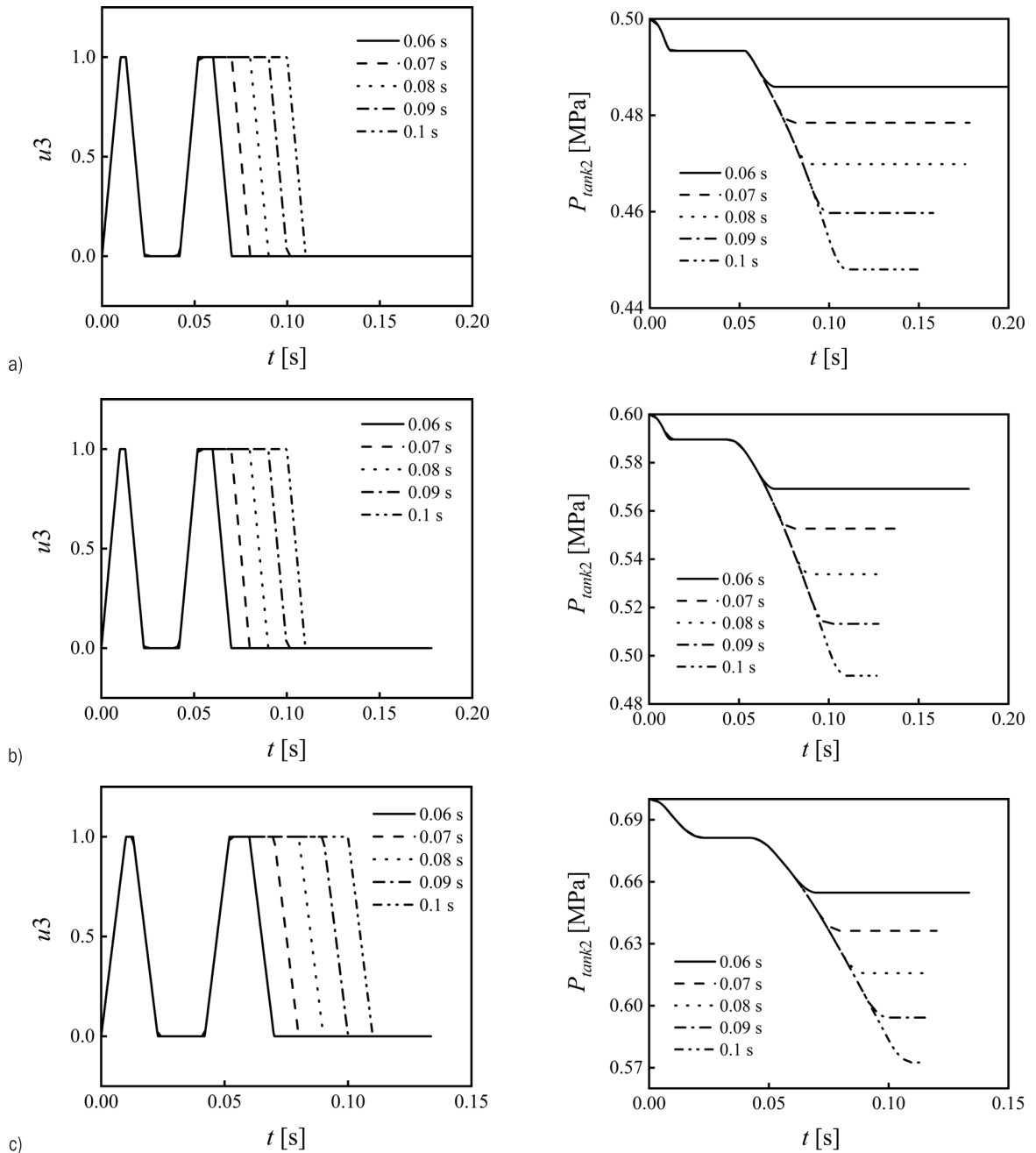


Fig. 11. The working condition of the solenoid valve and the initial pressure of tank2 is: a) 0.5 MPa, b) 0.6 MPa, and c) 0.7 MPa

5.3 System Performance Analysis of Variable Volumes of tank2

The initial pressure of tank2 is 0.6 MPa, the volume of tank2 is 0.8 L, 1 L, and 1.2 L, and cut off the compressed air supply of tank2 to the chamber b at 0.06 s, 0.07 s, 0.08 s, 0.09 s and 0.1 s, respectively. The expansion of the compressed air in the chamber b

can be utilized in the subsequent time. Fig. 14 shows the working conditions of the solenoid valve and the change of the pressure in tank2 in different working conditions.

It can be seen from Fig. 15 that when the volume of tank2 is constant, the energy saving efficiency decreases with the increase of the time of cutting off tank2, and when the time of cutting off tank2 is fixed,

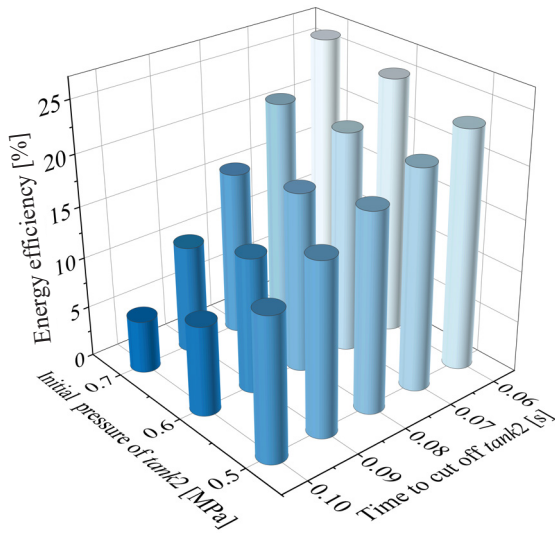


Fig. 12. Energy efficiency

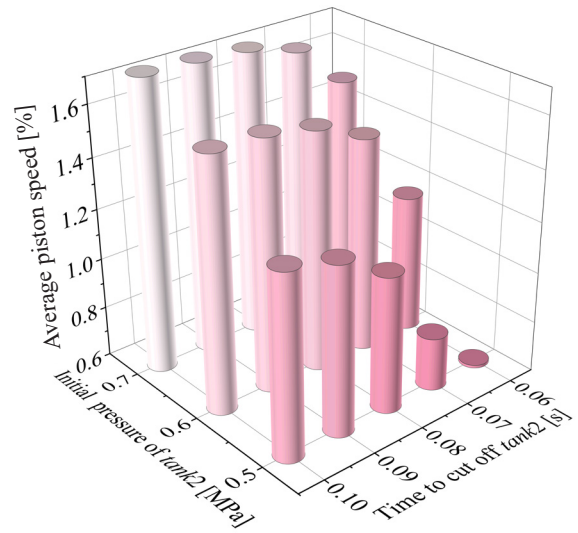


Fig. 13. Piston average speed

the average velocity of the piston decreases with the increase of the volume of *tank2*.

It can be seen from Fig. 16 that when the volume of *tank2* is constant, the average piston velocity increases with the increase of the time of cutting off *tank2*, and when the time of cutting off *tank2* is fixed, the average velocity of piston increases with the increase of *tank2* volume. This is because the increase in the volume of *tank2* leads to a decrease in pressure change, resulting in an increase in driving force.

When the initial pressure of *tank2* is 0.6 MPa, in order to improve the energy saving efficiency of the system and not make the piston speed too low affect the operation of the system, it is suggested that the time of cutting off *tank2* is 0.07 s to 0.08 s and the volume of *tank2* is 0.8 L to 1 L.

The difference in the compressed air supply time will make the expansion of the compressed air in the chamber *b* can be utilized to different degrees, but the piston speed will also be affected. The air supply time should be controlled to avoid the influence of the piston movement speed being too low on the system work.

6 CONCLUSION

To use the compressed air, this paper proposes a pneumatic actuator exhaust utilization system to return the compressed air to the compressed air tank and supply it under suitable conditions. The conclusions of this study are as follows:

1. A new exhaust utilization circuit is designed to recover and utilize compressed air.
2. The simulation results are in good agreement with the experimental results, which verifies the accuracy of the mathematical model of the system.
3. The operating characteristics of the system are mainly affected by the dimensionless parameters, such as natural period, effective piston area, chamber *b* area, initial of *tank2*, volume of *tank2*, and the criterion of compressed air supply switching.
4. Some parameters that have a greater impact on system characteristics are optimized. At the optimal parameters, the exhaust utilization efficiency of the system is 34.7 %.
5. Expansion energy can be further utilized by controlling the air supply time. By controlling the air supply time, when the initial pressure of *tank2* is 0.5 MPa, 0.6 MPa, and 0.7 MPa, the maximum energy-saving efficiency is 23.25 %, 24.99 %, and 26.12 %. When the volume of *tank2* is 0.8 L, 1 L, and 1.2 L, the maximum energy-saving efficiency is 30.01 %, 24.99 %, and 21.51 %.

Overall, the compressed air utilization system can recover and utilize compressed air well. During the working process, the system parameters should be selected and optimized according to the specific work requirements. This paper provides a new technical solution for compressed air recovery and utilization and a theoretical basis for subsequent improvement of system control.

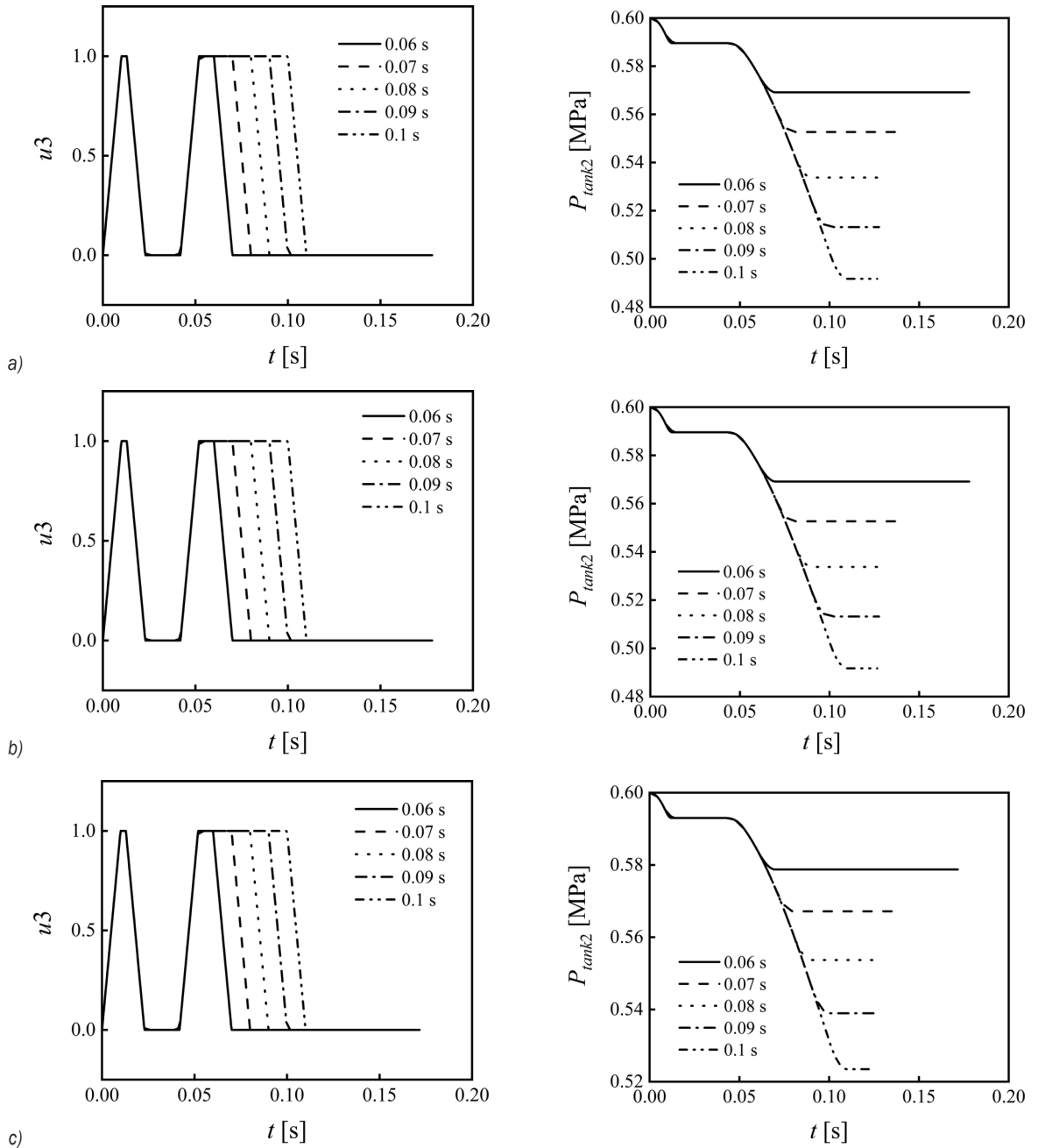


Fig. 14. The working condition of the solenoid valve and the pressure change in tank2 when tank2 volume is: a) 0.8 L, b) 1 L, and c) 1.2 L

7 ACKNOWLEDGEMENTS

The research work presented in this paper is financially supported by a Grant (52065054) from the National Natural Science Foundation of China and the Beijing Outstanding Young Scientists Program (BJJWZYJH01201910006021).

8 REFERENCES

- [1] Nazari, V., Surgenor, B. (2016). Improved position tracking performance of a pneumatic actuator using a fuzzy logic controller with velocity, system lag and friction compensation. *International Journal of Control, Automation and Systems*, vol. 14, p. 1376-1388, DOI:10.1007/s12555-015-0202-0.

- [2] Wang, J., Pu, J., Moore, P. (1999). A practical control strategy for servo-pneumatic actuator systems. *Control Engineering Practice*, vol. 7, no. 12, p. 1483-1488, DOI:10.1016/S0967-0661(99)00115-X.
- [3] Yusop, M.Y.M. (2006). *Energy Saving for Pneumatic Actuation Using Dynamic Model Prediction*. PhD Thesis. Cardiff University, Cardiff.
- [4] Du, H., Xiong, W., Xu, C., Jiang, Z. (2018). Direct drive system based on small gas compressor. *Chinese Hydraulics and Pneumatics*, vol. 2, p. 52-56. (in Chinese)
- [5] Krytikov, G., Strizhak, M., Strizhak, V. (2017). The synthesis of structure and parameters of energy efficient pneumatic actuator. *Eastern-European Journal of Enterprise Technologies*, vol. 1, no. 7(85), p. 38-44, DOI:10.15587/1729-4061.2017.92833.
- [6] Cai, M., Kagawa, T. (2001). *Energy Consumption Assessment of Pneumatic Actuating Systems Including Compressor*.
- [7] Du, H., Xiong, W., Jiang, Z., Li, Q., Wang, L. (2018). Energy efficiency control of pneumatic actuator systems through nonlinear dynamic optimization. *Journal of Cleaner Production*, vol. 184, p. 511-519, DOI:10.1016/j.jclepro.2018.02.117.
- [8] Du, H., Hu, C., Xiong, W., Jiang, Z., Wang, L. (2020). Energy optimization of pneumatic actuating systems using expansion energy and exhaust recycling. *Journal of Cleaner Production*, vol. 254, art. ID 119983, DOI:10.1016/j.jclepro.2020.119983.
- [9] Yang, F., Tadano, K., Li, G., Kagawa, T., Peng, J. (2016). Simulation on the characteristics of pneumatic booster valve with energy recovery. *Theory, Methodology, Tools and Applications for Modeling and Simulation of Complex Systems*. Springer, Singapore, p. 143-153, DOI:10.1007/978-981-10-2669-0_16.
- [10] Yang, F., Tadano, K., Li, G., Kagawa, T. (2017). Analysis of the energy efficiency of a pneumatic booster regulator with energy recovery. *Applied Sciences*, vol. 7, no. 8, art. ID 816, DOI:10.3390/app7080816.
- [11] Endler, L., De Negri, V.J., Castelan, E.B. (2015). Compressed air saving in symmetrical and asymmetrical pneumatic positioning systems. *Proceedings of the Institution of Mechanical Engineers, Part I: Journal of Systems and Control Engineering*, vol. 229, no. 10, p. 957-969, DOI:10.1177/0959651815597819.
- [12] Shi, Y., Jia, G., Cai, M., Xu, W. (2015). Study on the dynamics of local pressure boosting pneumatic system. *Mathematical Problems in Engineering*, vol. 2015, art. ID 849047, DOI:10.1155/2015/849047.
- [13] Shi, Y., Cai, M. (2012). Dimensionless study on outlet flow characteristics of an air-driven booster. *Journal of Zhejiang University SCIENCE A*, vol. 13, p. 481-490, DOI:10.1631/jzus.A1100176.
- [14] Tong, Z. (2021). Advancing Pneumatic Technology and Industry. *Hydraulics Pneumatics & Seals*, vol. 41, no. 02, p. 98-109. (in Chinese)
- [15] Beater, P. (2007). *Pneumatic Drives: System Design, Modelling and Control*. Springer, Berlin, DOI:10.1007/978-3-540-69471-7.
- [16] Doll, M., Neumann, R., Sawodny, O. (2011). Energy efficient use of compressed air in pneumatic drive systems for motion tasks. *Proceedings of International Conference on Fluid Power and Mechatronics*, p. 340-345, DOI:10.1109/FPM.2011.6045785.
- [17] Doll, M., Sawodny, O. (2010). Energy optimal open loop control of standard pneumatic cylinders. *7th International Fluid Power Conference*, Aachen, p. 259-270.
- [18] Cummins, J.J., Barth, E.J., Adams, D.E. (2015). Modeling of a pneumatic strain energy accumulator for variable system configurations with quantified projections of energy efficiency increases. *Proceedings of the ASME/BATH Symposium on Fluid Power and Motion Control*, DOI:10.1115/FPMC2015-9605.
- [19] Luo, X., Wang, J., Sun, H., Derby, J.W., Mangan, S.J. (2012). Study of a new strategy for pneumatic actuator system energy efficiency improvement via the scroll expander technology. *IEEE/ASME Transactions on Mechatronics*, vol. 18, no. 5, p. 1508-1518, DOI:10.1109/TMECH.2012.2203920.
- [20] Cai, M. (2007). Theory and practice of modern deterministic techniques, Lecture 4: Energy of compressed gas. *Hydraulics Pneumatics and Seals*, vol. 5, p. 54-59. (in Chinese)
- [21] Shi, Y., Cai, M. (2013). Dimensionless study on output flow characteristics of expansion energy used pneumatic pressure booster. *Journal of Dynamic Systems, Measurement, and Control*, vol. 135, no. 2, art. No. 021007, DOI:10.1115/1.4007234.
- [22] Yu, Q., Cai, M., Shi, Y., Xu, Q. (2015). Optimization study on a single-cylinder compressed air engine. *Chinese Journal of Mechanical Engineering*, vol. 28, p. 1285-1292, DOI:10.3901/CJME.2015.0520.072.
- [23] De Wit, C.C., Olsson, H., Astrom, K.J., Lischinsky, P. (1995). A new model for control of systems with friction. *IEEE Transactions on Automatic Control*, vol. 40, no. 3, p. 419-425, DOI:10.1109/9.376053.
- [24] Harris, P., Nolan, S., O'Donnell, G.E. (2014). Energy optimization of pneumatic actuator systems in manufacturing. *Journal of Cleaner Production*, vol. 72, p. 35-45, DOI:10.1016/j.jclepro.2014.03.011.
- [25] Yu, Q., Zhai, J., Wang, Q., Zhang, X., Tan, X. (2021). Experimental study of a new pneumatic actuating system using exhaust recycling. *Sustainability*, vol. 13, no. 4, art. ID 1645, DOI:10.3390/su13041645.
- [26] Shi, Y., Cai, M. (2011). Working characteristics of two kinds of air-driven boosters. *Energy Conversion and Management*, vol. 52, no. 12, p. 3399-3407, DOI:10.1016/j.enconman.2011.07.008.
- [27] Yu, Q., Hao, X., Tan, X. (2018). Performance analysis of an innovative kind of two-stage piston type expansion air engine. *Advances in Mechanical Engineering*, vol. 10, no. 5, art. ID 1687814018773860, DOI:10.117/1687814018773860.